Science and Technology Indonesia
e-ISSN:2580-4391 *p*-ISSN:2580-4405
Vol. 11, No. 1, January 2026

Research Paper

Optical Assessment of Titanium Oxide Employed in Phosphor-Transmuted WLED Devices

Phan Xuan Le[1], Nguyen Thi Phuong Loan[2], Nguyen Doan Quoc Anh[3*]

[1]*Faculty of Electrical Engineering Technology, Industrial University of Ho Chi Minh City, Ho Chi Minh City, 70000, Vietnam*
[2]*Faculty of Fundamental 2, Posts and Telecommunications Institute of Technology, Ho Chi Minh City, 70000, Vietnam*
[3]*Faculty of Electrical and Electronics Engineering, Ton Duc Thang University, Ho Chi Minh City, 70000, Vietnam*
***Corresponding author**: nguyendoanquocanh@tdtu.edu.vn

Abstract
Utilizing inexpensive PbO-B_2O_3-SiO_2-ZnO glass as the host, a new environmentally friendly method for phosphor-transformed WLED utilizing Ce:YAG-doped glass and Titanium oxide (TiO_2) was effectively created for this study. This method demonstrated good sintering behavior and elevated visible transparency with a sintering heat level reaching 750°C while avoiding influence on phosphor samples. The optic characterization of WLED can be simply adjusted by only modifying the temperature, incorporating dosage, as well as sample breadth to suit the mucous sintering for phosphor within glass (PwG). The perfect sample amount is regulated, reaching 5 wt.% of the end combination, and the most suited thickness of samples is discovered to be 0.8 mm. As a consequence, the optimum heating condition is sintered at 700°C within 40 minutes. The built-in PwG WLED displays an elevated illuminating effectiveness of 134.33 lm/W, associated hue temperature of 4696 K, and hue rendering index of 68.5. PwG's improved heat quenching ability when combined with traditional silicone resin and TiO_2 makes it clear that the glass ceramic substance used today is highly practical for use in WLED apparatuses.

Keywords
LED Lamps, $CaSr_2(PO_4)_2:Eu^{3+}$, X-Ray Diffraction, CIE Hue Coordinates, Luminous Efficacy

Received: 17 June 2025, Accepted: 20 December 2025
https://doi.org/10.26554/sti.2026.11.1.345-355

1. INTRODUCTION

Owing to its significant significance in technological usage to be a novel generation solid-state illumination supply and the exceptional requires in many areas, including long lifespan, energy efficiency, and environmental friendliness, diode emit white illumination (WLED) has been the focus of extensive research throughout recent years (Qiang et al., 2025; Fang et al., 2025; Cong and Anh, 2025). Although this is going on, efforts are being made to develop WLEDs that have qualities such as elevated luminous effectiveness (LE), adjustable correlated hue temperature (CCT), elevated hue rendering index (CRI), and long-term reliability that are greater to those of conventional illumination supplies (Anh and Ngoc, 2020; Zhou et al., 2024). Additionally, it is anticipated to be a strong contender for a solid-state illumination supply that can eventually replace incandescent or fluorescent lights.

To the best of our understanding, a solid-state semiconductor gadget called an LED (light-emitting diode) can transform electrical power straight into illuminating power. Organic silicone surrounds a semiconductor chip called LED (Kumar and Kumar, 2024). The cathode of the chip is the end that connects to a bracket, and the anode is the end that is linked to the power source. Thus, it comprises an n-kind semiconductor, which is driven by electrons, connecting with a *p*-kind semiconductor, which is controlled by holes. The chip emits photons when current flows across it, pushing electrons into the *p*-kind region and recombining them with holes in the p-n junction area. A valence range is produced by the anode, whereas a conductive range is produced by the cathode (Zhang et al., 2024; Chen and Huang, 2024). Among them, a band space (forbidden band) would manifest. In the *p*–*n* junction area, the re-mixing of electrons and holes produces power that is emitted as photons. The development of the *p*–*n* junction determines the frequency (hue) of the produced illumination (Tran et al., 2020).

To create white illumination from blue LEDs, a number of techniques have been suggested. Ce:YAG granules are mixed within natural silicone as well as applied to blue chips in commercial devices (Markovskyi et al., 2024; Le et al., 2021). Phosphors absorb some of the blue illumination, which is then partially released as yellow illumination; the remaining amount is transferred. White illumination is created when blue as well

as yellow rays are combined. The support of phosphor granules by matrix components is crucial in order to evenly spread the particles over the LED chips to create a steady formation. Curable silicone is now the most often used carrier substance for phosphors in wavelength changers due to its elevated optic transmission and low fabrication heat. Nevertheless, due to the organic silicone's low glass transformation heat, UV light and heat over 150°C damage it, turning the generated hue yellow and producing a significant drop in transmission. As a result, the yellowish organic silicone impairs the optic capabilities of WLED, as seen by lumen loss and hue change. It, therefore, becomes needed for creating novel silicone-free heating-steady phosphor carriers for use in elevated-energy WLEDs (Wang et al., 2024; Chan et al., 2024).

Ce:YAG glassy ceramic (CGC), the novel luminous substance that contains nano-/micro-crystalline granules concentrated through preliminary glassy substances through carefully regulated crystallizing process, is utilized in place of the traditional silicone-derived phosphor conversion when it comes to building elevated-energy WLEDs. It is a significant material with great heating resistance and ease of shaping, and it may concurrently be employed as an encapsulating substance and luminous convertor in phosphor-transformed WLEDs. Remarkably, this GC-based WLED displays show lower degradation than silicone-based WLED in terms of maximum emitting strength, hue change, lumen loss, transmission loss, and resistance to heating deterioration, heating shock, and damp heat (Xu et al., 2024). Consequently, glass crystallization technique and low-heat co-sintering are the two primary synthesizing routes for creating CGC phosphors. The first method has many benefits, including portability, affordability, and the ability to create a variety of phases and configurations by creating a suitable glass composition and crystallization, but it additionally comes with numerous drawbacks, including constructed uncertainty of the glass and the need to exactly regulate crystallizing conditions. The WLED's LE accompanied by CGC merely reached 52.20 lm/W because partitioning every Ce^{3+} triggers within the YAG base throughout its crystallizing process as well as achieving elevated translucency are challenging (Liu et al., 2024). The other offers numerous benefits, including a lower sintering temperature and the ability to combine different commercial phosphor powders with glasses. Chen and Wang most lately used the joint-sintering process under small heat level for creating CGCs yielding an elevated QY reaching 92%. Because pricey TeO_2 is used as the primary glass element in this technique, the issue of its expensive expense still exists. Additionally, the preparing technology is complex and requires two procedures. In this section it becomes necessary to design a new, straightforward, and workable technique and increase specimen transparency in order to enhance the LE for CGC samples (Zeng et al., 2025).

The research herein focuses on creating translucent CGCs that can be utilized as yellow phosphors for WLEDs using a previously unreported sole-stage low-temperature co-sintering process. Ce:YAG samples and glassy powder samples possessing elevated refractivity indices were combined to create compounds. The viscous sintering of the compound substances has been tailored for the heating circumstance, incorporating dosage, and sample breadth. The co-sintered mixes' microstructures and local compounds were examined. Additionally included were CGCs' optic characteristics and crystalline procedure (Liu et al., 2025). Compared to an earlier work by, which employed SZSPOE as scattering material, the Ce:YAG-integrated PwG samples yield greater scattering coefficients under high wavelengths, more consistent CCT outcomes across various particles sizes, and smaller CRI and CQS reduction as the particle size increases.

2. EXPERIMENTAL SECTION

2.1 Chemical and Procedure

Glass frits and Ce:YAG samples were combined into a mixture containing $47PbO–35B_2O_3–7SiO_2–11ZnO$ (mol%). The frits possess a small softening degree, advantageous in preventing unforeseen phosphor degradation during thermal treatment. Additionally, this glass has a refractive index of 1.81, which is comparable to the 1.83 for Ce:YAG. Since the entire inner reflection at the interface results in a loss of illuminating effectiveness, it is crucial to fit the refractive indices of the two mediums. In the years to come, PbO has to be substituted with an environmentally safe element (Jiang et al., 2025). To create homogenous particles, Ce:YAG were utilized directly under no further processing, with the end result's phosphor powder content being adjusted, reaching 3 wt.%, 5 wt.% as well as 7 wt.%. In an agate mortar, these mixes were homogenously combined and pulverized for one hour. Following that, they were sintered under various heating conditions within a furnace, lasting anywhere from 20 minutes to 60 minutes at temperatures between 650 and 750°C. To regulate the finished thickness of the sintered examples, 100 g loads were utilized during the sintering process. Details on instruments used for characterizing the samples are detailed below.

2.2 Instrumentation and Characterization

Every sample was dual-plane polished. The crystalline formation for the sampling units was assessed via X-ray diffracting utilizing D8 Focus Bruker from Germany under Cu subject, a quickening voltage reaching 40 kV, as well as a scanning span between 20° and 80° with a scanning step reaching 0.02 (°)/s. The form as well as magnitude for the sampling units were assessed via field-discharge scanning electron microscopic assessment utilizing FEI Nano SEM 200 apparatus (Li et al., 2024). The photoluminescence (PL) spectra as well as PL lifetime degradation arch of the samples were assessed via one FluoroMax-4 spectrophotometric apparatus from HORIBA Jobin Yvon. The optical attributes were examined via one incorporating globe PMS-50, Everfine from China, subject to a forward bias reaching 20 mA. Every assessment was conducted under room temperature.

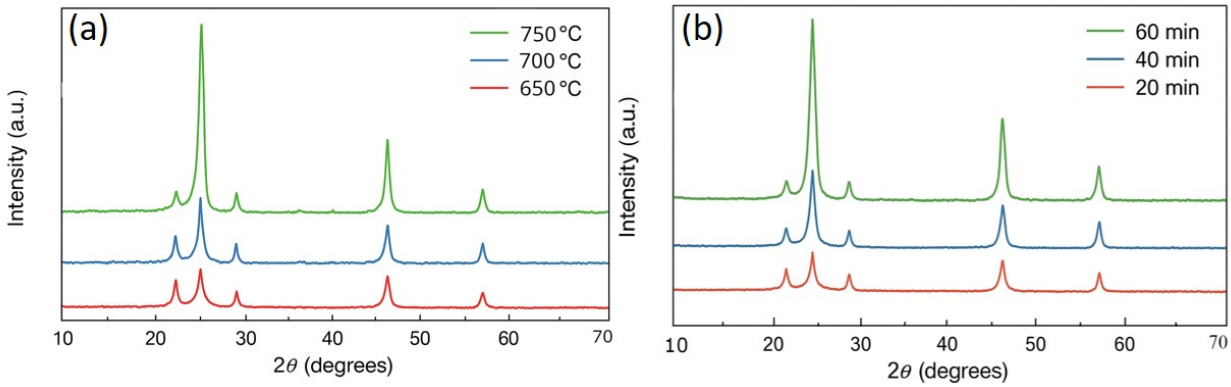

Figure 1. XRD Profile of Ce:YAG

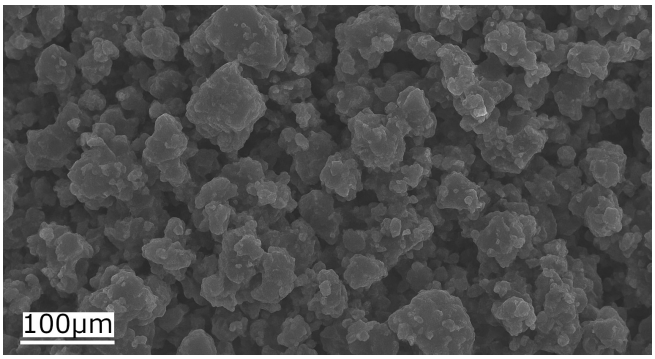

Figure 2. SEM Visual of Ce:YAG

3. RESULT AND DISCUSSIONS

3.1 Attribute Analysis

The stage clarity as well as crystalline structure for the acquired samples subject to sintering process under disparate thermic state was examined via XRD assessments. According to Figure 1, the XRD profile for Ce:YAG phosphor sample is compatible with the conventional card (JCPDS No. 33–0040), suggesting that the sample undergoes desirable crystallization (Zhao et al., 2015). Posterior to integrating said sample unto the glass laticework, illustrated via Figure 1(a), the XRD apexes for the acquired samples subject to sintering process under 650°C within forty minutes or 700°C within forty minutes would resemble the conventional YAG granule (JCPDS No. 33–0040). Impure apexes are absent. Regardless, as the sample undergoes a sintering process under 750°C within forty minutes, the quantity of XRD apex declines (Gong et al., 2015). Afterwards, based on Figure 1(b), as the synthesized samples undergo a sintering process under 700°C within fifteen, forty as well as fifty-five minutes, every XRD apexes would resemble the conventional YAG granule, showing that the phosphor possesses desirable thermic attribute as well as the ability to withstand significant heat level under 700°C (Lü et al., 2015). Additionally, every sample displays a glassy status (Qin et al., 2024).

The SEM visual for the synthesized samples subject to the sintering process under heat levels between 650°C and 700°C within forty minutes as well as temporal units between fifteen and fifty-five minutes under 700°C is displayed via Figure 2, where the synthesized samples display desirable translucency. The significant optic translucency for said samples results from the significant refraction indicator from the PBSZ glassy base resembling Ce:YAG. Subsequently, a small illumination dispersion penalty manifests, proving challenging for application to regular slurry due to the uneven allocation for phosphor within the organic sap (Long et al., 2020). With the extension in the sintering heat as well as temporal unit, the sample chroma is altered between vivid yellow and faint yellow since the phosphor would merely withstand a strong heat of 700°C within a specific period, in agreement with Figure ??. Afterwards, the intrinsic micro-formation as well as granule allocation for the sampling units would be noteworthy, displayed via Figure 2, the phosphor samples would be seemingly integrated within the glassy latticework proficiently while avoiding observable crevices as well as inconsistencies. Since supplementary processing would not be conducted upon Ce:YAG, the form as well as magnitude allocation for the phosphor granules would be uneven (Huang et al., 2015). The superior homogeneity for the powdered phosphor allocated within the glassy latticework is displayed via Figure ??. Notably, the quantity of phosphor granules declines under surging sintering heat, caused by the severe corrosion for the phosphor via the liquifying glass featuring particularly substantial sintering heat (Won et al., 2011). As such, smaller sintering heat proves paramount for developing CGC with desirable luminescent attributes. As a result, the desirable thermic state would be preliminarily deemed 700°C within forty minutes.

For additional validation, the PL as well as PLE spectra for the synthesized samples would be identified and displayed via Figure 3. The PLE spectra for the synthesized samples exhibit one wide exciting band focalized under roughly 400 nm and one exciting band found under roughly 350 nm caused by the 4f–5d shift for Ce^{3+}, as displayed via Figure 3(a) and (c), respectively. Additionally, as the synthesized samples are subject to blue illumination exciting process under 400 nm, they would

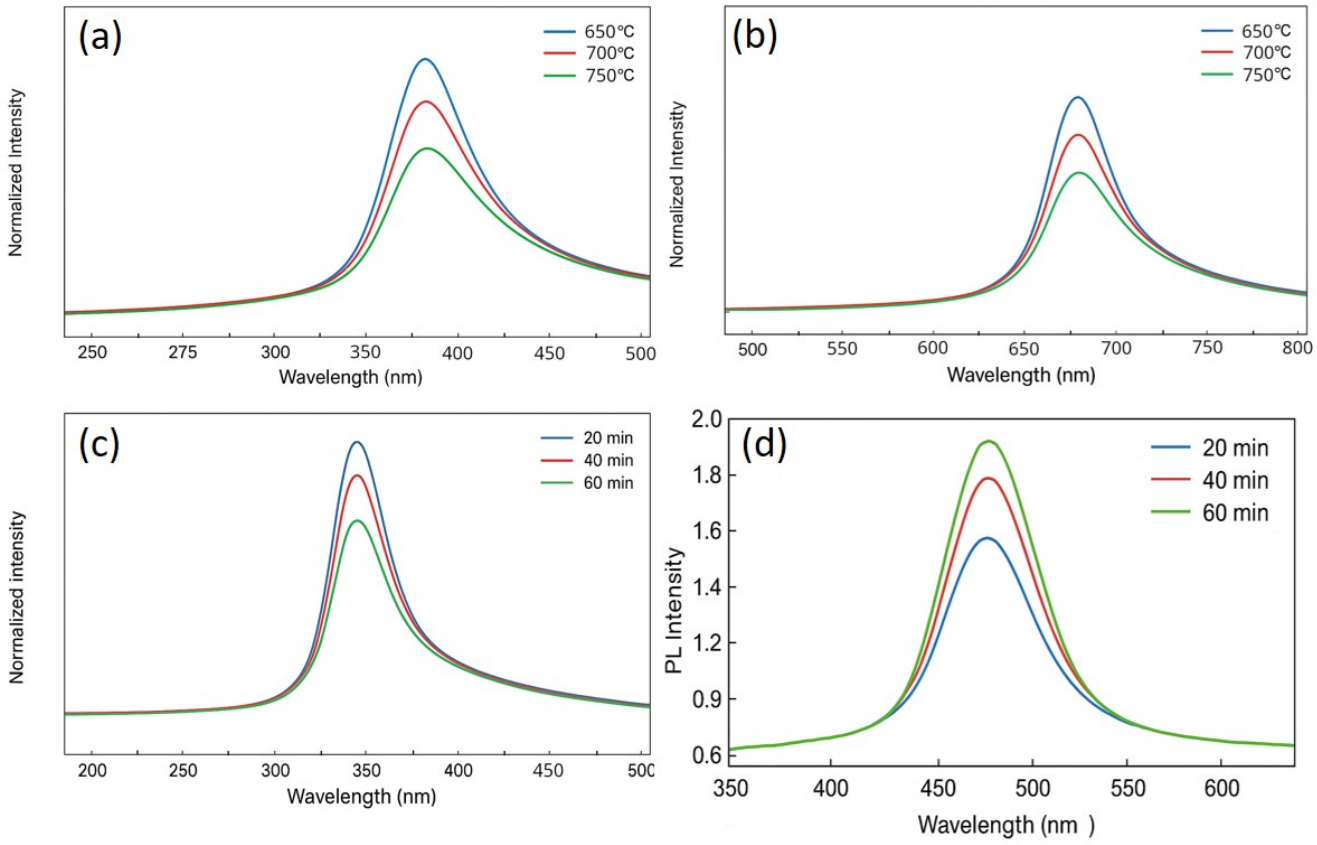

Figure 3. PLE and PL Spectra of the Ce:YAG PwG Sintered (a) and (b) at Different Temperatures for 40 Minutes, (c) and (d) Sintered at 700°C for Different Periods

display a conventional Ce^{3+}: 5d–4f discharge band focalized under 680 nm, displayed via Figure 3(b), resembling the powdered Ce:YAG (Lv et al., 2017). Regardless, the exciting as well as discharge intenseness show substantial variance. Based on Figure 3(a), the exciting intenseness would decline when the sintering heat surges. According to 3(c), it initially surges then declines as the wavelength increases. In relation to time periods, it declines when the sintering process goes on (Das et al., 2018). Based on 3(b) and (d), the discharge intenseness would initially surge then decline as the wavelength becomes greater. In 3(b), the intenseness goes down as the sintering heat increases, while in 3(d), the intenseness is proportional to the advancing sintering process. When the sintering heat remains under 750°C within forty minutes, the discharge apex found under 680 nm exhibits a minor shift, possibly resulting from the substantial influence from the strong heat upon the formation as well as attributes for Ce:YAG (Samanta et al., 2015).

3.2 Influence of Sintering Condition on PwG

The as-prepared samples' PL degradation characteristics are additionally investigated. The as-prepared samples demonstrate, as predicted, that the sole-exponential function listed below matches the deterioration behavior more effectively, surpassing dual-exponential as well as threefold counterpart (Hu et al., 2018):

$$I(t) = I(0)\exp(-t/\tau) \quad (1)$$

where τ is the radiation degradation period, $I(t)$ and $I(0)$ signify the luminous strengths under temporal unit t and 0, correspondingly.

In the case of sintering heats reaching 650, 700, as well as 750°C along with corresponding sintering heat times reaching 20, 40, as well as 60 minutes, the connections provide degradation times of almost 57.92 ns. Among the properties for the Ce^{3+} electric-dipole permitted 5d–4f transformation is degradation period in the millisecond range (Wang et al., 2015). It is noteworthy to acknowledge that the degradation behavior of the samples as they were prepared matches the rate for Ce:YAG degradation, resulting in one degradation duration reaching 58.25 ns, demonstrating the possibility for $PbO–B_2O_3–SiO_2–ZnO$ latticework to become the optimal base and the relatively small Ce:YAG degradation throughout glassy thawing for the current setup with its sintering condition of 750°C. For CGCs, Ce^{3+} granules may assume the YAG lattice's dodecahedron

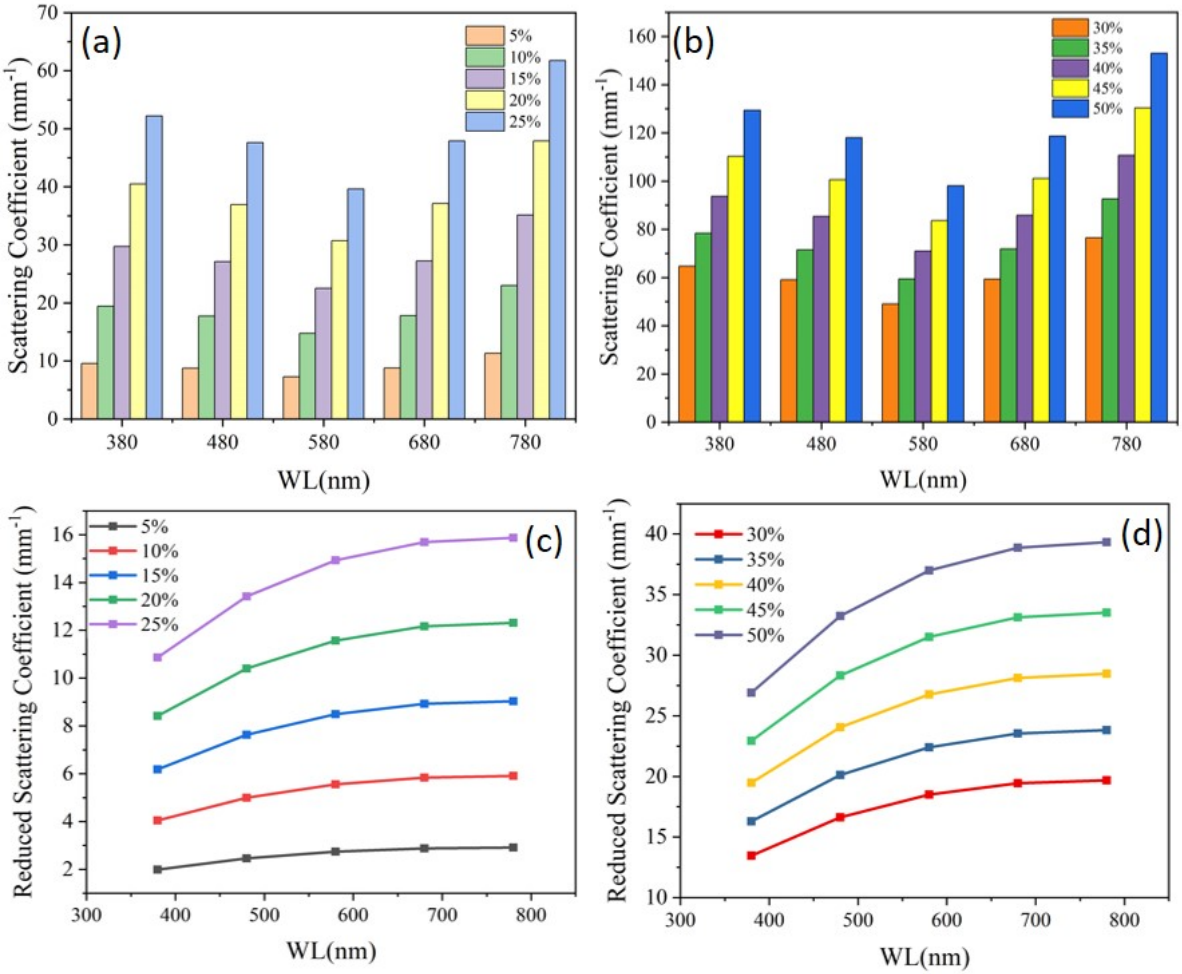

Figure 4. Scattering Coefficients (a, b) and Reduced Scattering Coefficients (c, d) with Various TiO_2 Levels

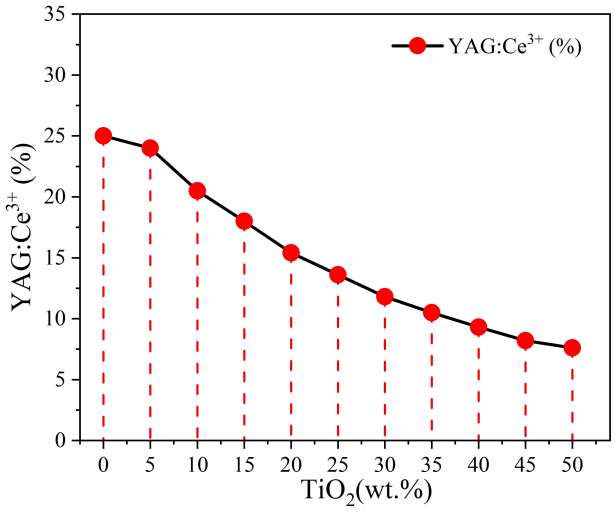

Figure 5. YGA:Ce Under Disparate TiO_2 Dosages

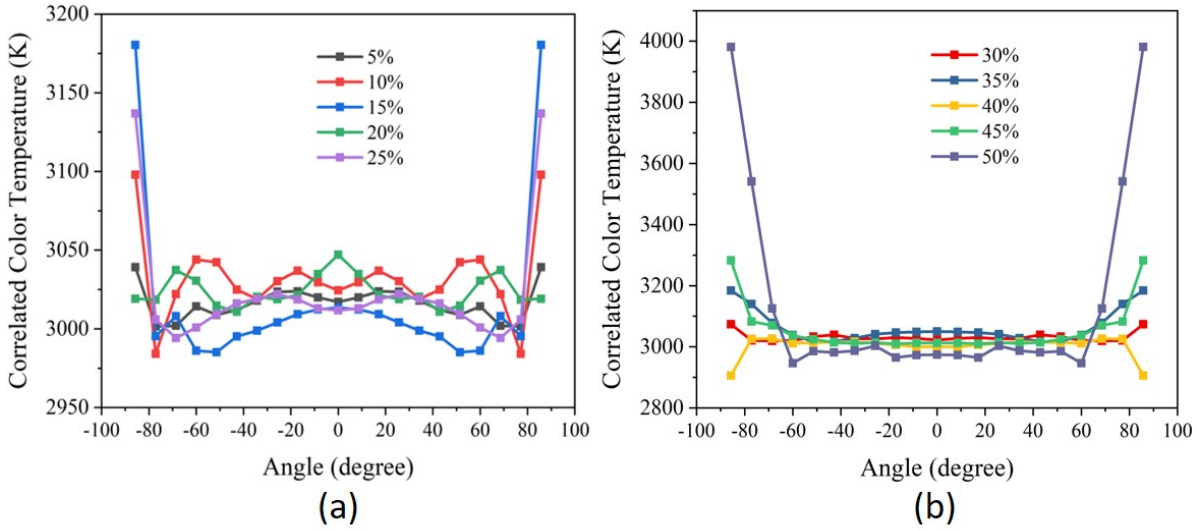

Figure 6. CCT Values with Various TiO_2 Levels: (a) 5%–25%; (b) 30%–50%

position to replace Y^{3+} ions, and the crystal field's strength causes a significant crystal-field splitting in Ce^{3+}'s 5d structure (Meejitpaisan et al., 2022). The 4f–5d transformation for Ce^{3+} moves towards the observable area as a consequence, moving the lowest 5d level lower in space. The initial permitted 4f–5d transformation for Ce^{3+} granules, between the 4f state ($2F_{5/2}$) and foundation 5d state ($2A_{1g}$), is thought to be the cause of the stimulation range centered at 460 nm (Tang et al., 2018). The second permitted 4f–5d transformation, 4f ($2F_{5/2}$)–5d ($2B_{1g}$), is what causes the shoulder stimulation maximum at 340 nm. This is consistent with the findings described in the literature (Won et al., 2011). The emitting range with a center at 540 nm is made up of emitting ranges with centers under 560 as well as 520 nm, accordingly, explained by Ce^{3+} transitions between 5d ($2A_{1g}$) and 4f as well as between 5d and 4f (Zhao et al., 2010; Fang et al., 2014). It proves vital to select the optimal heating setting for preparing samples that are utilized to encapsulate WLED because unanticipated phosphor deterioration that appears during thermal treatment makes this decision essential (Camargo et al., 2022). Utilizing one incorporating globe and specific electrical fluxes, their optic characteristics are assessed. When flux (I) rises between 20 and 60 mA, the samples' LE is seen to trend decrease. When sintered at 700°C for 40 minutes, the LE of the as-prepared sample achieves its highest point. When heats are too elevated or retention times are too long, Ce:YAG phosphor may unexpectedly degrade, which will negatively impact the optic efficacy of the samples as-prepared (Huang et al., 2024).

Our samples under a range of breadth (0.6–1.0 mm) would be shown with their CIE hue coordinates. The hue coordination changes between a green-yellow and a blue area while the sintering heat rises. When the sintering duration grows, the color coordination transitions between the blue and the yellow region (Wang et al., 2018). Our as-prepared samples' thickness rises with their alignment as both x and y grow. Thus, selecting samples produced with optimum heat conditions to encapsulate WLED grows more and more attractive in order to gain elevated-quality white illumination (Shrivastava and Kundu, 2023). As was already noted, a number of phenomena indicate that the sample that was manufactured as is and subject to sintering under 700°C within forty minutes under 0.8-mm breadth would be the most acceptable (Dong et al., 2020). One CGC panel was embedded onto one blue chip to create the GC-WLED device as a proof-of-concept experiment. The electroluminescent (EL) spectral factor for the chip displays one blue range under about 460 nm, whereas said factor in the WLED with CGC shows one blue emitting range as well as yellow emitting range, resulting in white discharges generated by the 5d–4f transformation from Ce^{3+} (Li et al., 2019). The LE of as-prepared samples rises first before declining while

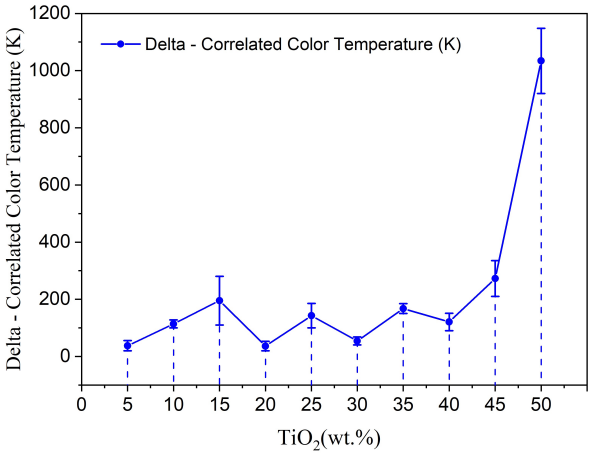

Figure 7. Chroma Disparity under Disparate TiO_2 Dosages

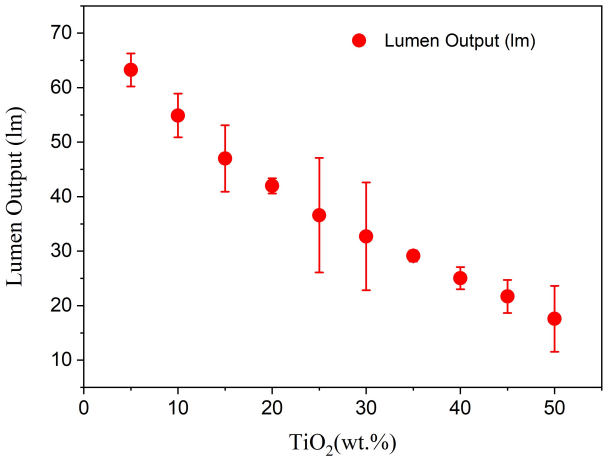

Figure 8. Luminescence Strength with Various TiO_2 Levels

the sintering heat level rises because the blue radiation portion reduces firstly followed by rises at the same time as the yellow emitting portion rises firstly before declining. It is noteworthy to see that while the CRI keeps rising, the CCT initially declines before rising. Additionally, if the sintering time extends, the EL spectral factor exhibits the same changing behavior, with the exception that the CRI lowers initially before increasing (Hop et al., 2024). The blue radiation element attains its lowest point and the yellow radiation element mixed with the blue emission element gets to its highest point when the heating condition is set at 700°C for 40 minutes. This results in greater white illumination emitting than under other conditions, additionally demonstrating that this is the optimal heating condition.

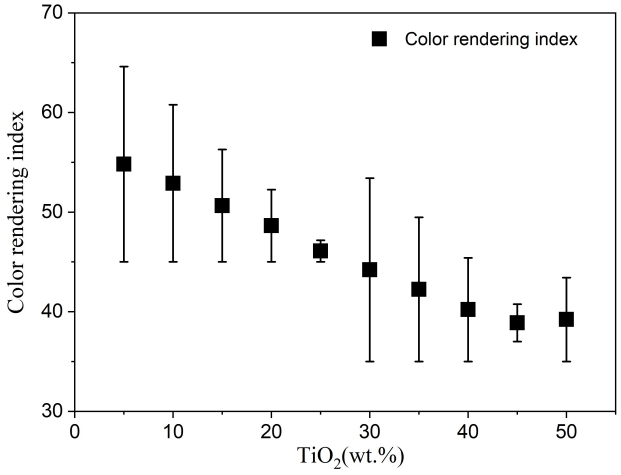

Figure 9. CRI under Disparate TiO_2 Levels

3.3 Assessment of Optical Characteristics under Titanium Oxide

Figure 4(a) shows the dispersion coefficient as well as decreased dispersion coefficient, whereas Figure 4(b) exhibits the connection between the dosage of TiO_2 and the dispersion of light. It allows for higher TiO_2 doses by enhancing illumination transference as well as wavelength transmutation proficiency. Brightness might rise if forward emission blue light dispersion increased and forward scattering and reabsorption of blue light decreased (Wang et al., 2018). To do this, we need to increase the TiO_2 content while decrease the yellow phosphorus content (Yue et al., 2022). The associated chroma heat level (CCT) is less likely to vary at the same time. Figures 6 and 7 show that CCT is not concentration-dependent, unlike Figure 5, which shows that the dosage of YGA:Ce decreases as the dosage of TiO_2 increases (Ma et al., 2024). Figure 5 shows that the TiO_2 doses range from 25–35% if the YGA:Ce proportions prove smaller, ranging from nearly 12% to just over 10%. Increasing the amount of doping might lower the phosphor's CCT variance, as seen in Figure 6. At around 3200 K, the CCT values are maximum for a 35% TiO_2 solution. On the other hand, the result at 35% TiO_2 with a D-CCT value of over 200 K is approximately 150 K higher than the D-CCT value at 30% TiO_2, as shown in Figure 7.

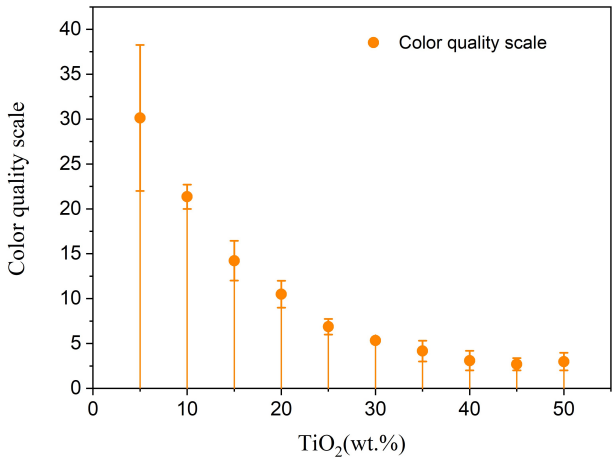

Figure 10. CQS under Disparate TiO_2 Dosages

Figure 8 shows that there were cases when the white light emission was not brighter after adding TiO_2. The outcomes with 25% TiO_2 were optimal, whereas those with 35% TiO_2 were subpar. This displays an uneven distribution of hues and a decrease in blue emission as a result of enhanced backscattering and reabsorption (Zhu et al., 2015). For example, increasing the percentage of TiO_2 would cause a transition for the phosphor between blue and yellow or orange-red under influence from additional rear-reflected blue illumination. Certain concentrations of TiO_2 are necessary prior to the expansion of the sample's coating (Motloung et al., 2015). Multiple reflections of the altered light from different objects would limit the emission spectrum. As such, although a high phosphor dosage may improve CCT, it may reduce luminous intensity via boosting the amount for rear-reflected transmuted illumination (Chen et al., 2019). Figure 8 shows that a 25% TiO_2

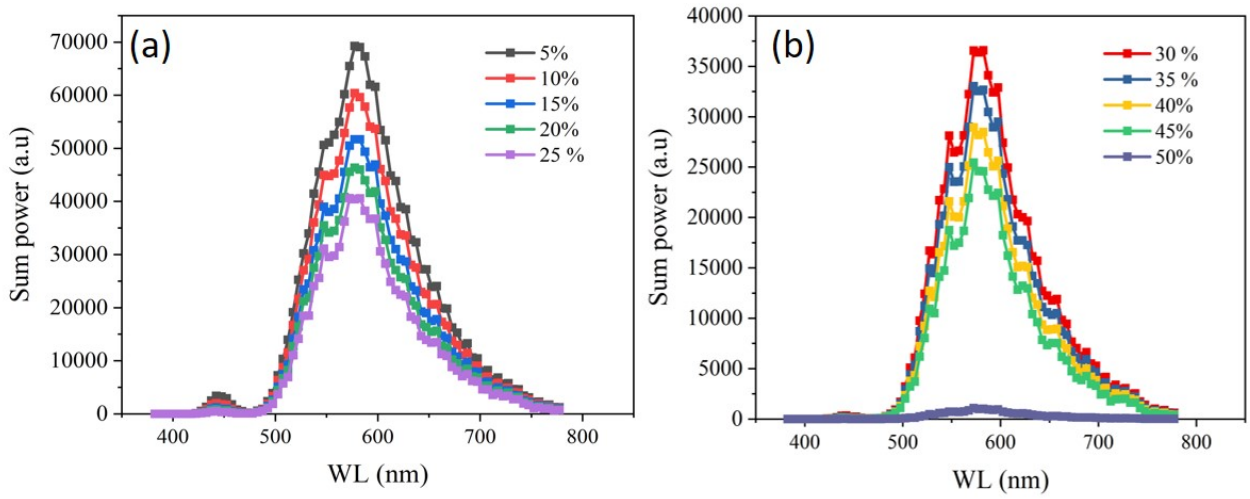

Figure 11. Luminescence Power of the WLED: (a): 5%-25%; (b): 30%-50%

Table 1. Result Comparison of Scattering Coefficients Influenced by Particle Sizes of Scattering Materials

Scattering Materials	Scattering Coefficients (mm^{-1})	Reduced Scattering Coefficients (mm^{-1})	References
TiO_2	92.7	23.8	This work
ZnO	80.3	11.4	(Cong et al., 2024)
KBr	42.5	13.5	(Anh et al., 2025)
$CaCO_3$	8.96	0.15	(Tung et al., 2024)

Table 2. Comparative Tables of this Research Results with Reported Research

Scattering Materials	YAG:Ce^{3+} (%)	CCT (K)	D-CCT (K)	CRI	CQS	Lumen (lm)	References
TiO_2	13.6	3000	54.2	46.1	6.9	36.6	This work
ZnO	7.5	5000	40.8	58.1	62.4	146.6	(Cong et al., 2024)
KBr	27.4	3000	35.4	56.2	42.4	73.7	(Anh et al., 2025)
$CaCO_3$	5.95	6000	460	60.8	62.6	173.2	(Tung et al., 2024)

percentage was found to be enough with over 35 lm of lumen output power to improve the simulated WLED's brightness and color uniformity.

Figures 9 and 10 demonstrate that the amount of TiO_2 greatly affects how white LEDs seem and how accurately colors are reproduced. As the TiO_2 concentration rose to 35%, color rendition studies using the CRI along with chroma quality scale (CQS) displayed a uniform decrease. The aforementioned components may seem to be declining if the proportions of blue, green, and yellow-orange are inconsistent (Milisavljevic et al., 2022). Increased TiO_2 levels not only improve dispersion, but also produce a skewed light emission that leans toward the yellow-orange spectrum. It is necessary to modify the CRI and CQS for our phosphor; other factors, including particle size, would come into consideration during data analysis (Wei et al., 2019).

For validation testing, one CGC WLED apparatus was built via encasing one Ce:YAG CGC disc upon one blue chip. The EL spectra for the chip exhibits one blue-discharging band under roughly 460 nm, whilst the EL spectra for CGC WLED displays one blue discharge band as well as yellow counterpart, generating white illumination caused by the 5d–4f of Ce^{3+}. With the sintering heat surging, the blue discharge element preliminarily declines then surges, whilst the yellow discharge element preliminarily surges then declines, causing the LE for the synthesized samples to preliminarily surges then declines (Lin et al., 2014). Notably, the CRI proceeds with surging, whilst the CCT preliminarily declines then surges. In addition, with the sintering process progressing, the EL spectra exhibit identical shifting tendency. However, the disparity would be that the CRI preliminarily declines then surges. As the selected thermic state is under 700°C within forty minutes, the blue discharge element assumes its nadir value, the presence of yellow discharge element merged with blue discharge element assumes its peak value, subsequently generating additional white illumination compared to other states, validating that it would be the

desirable thermic state (Shen et al., 2024).

Additionally, one phosphor-integrated WLED was built utilizing one exterior-fixed InGaN blue chip. As the synthesized samples are merged with the chip subject to functioning under 20 mA, a segment of blue illumination would be subject to absorptivity via the samples then discharged again in the form of yellow illumination while the rest would be propagated (Yan et al., 2017). The merger between said blue as well as yellow rays generates white illumination. Notably, the LE as well as CCT would be substantially augmented under surging PwG disc breadth as well as phosphor-integrated dosage, primarily because of additional blue illumination subject to absorptivity leading to additional yellow illumination discharged (Pathak et al., 2016). Subsequently, the yellow-blue proportion would surge while the acquired luminescent chroma leans toward warm white then eventually yellow illumination with the resulting decline in CCT. In the meantime, the CRI declines when the Ce:YAG-integrated dosage as well as PwG breadth surge. According to the general assessment for the optic characteristics above, the optimal phosphor dosage would be 5 wt.% while the optimal PwG breadth would be 0.8 nm (My et al., 2022; Anh et al., 2025).

Figure 11 displays the TiO_2 discharge bands for various particle sizes. Across the whole white light spectrum, the TiO_2 may enhance blue and orange-red light, as shown. To improve the efficiency of lighting, one may manipulate the properties of TiO_2 to vary the profile for illumination absorption and scattering (Chen et al., 2021). The most intense peaks are seen in the blue (450 nm) along with yellow-orange (roughly 600 nm) wavelength band patterns. See Tables 1 and ?? for a comparison of the optical properties affected by particle size in this work with those in previous investigations using metal oxides or luminous phosphors (Cong et al., 2024; Tung et al., 2024).

4. CONCLUSIONS

In conclusion, the joint-sintering method under small heat level was effectively used to create translucent CGCs in just one stage. In the current system, an economical, PbO-B_2O_3-SiO_2-ZnO with significant refractivity indicator is produced in the form of the base with the aim of distributing Ce:YAG. CGCs can display distinct optic efficiency depending on the heating setting, incorporating proportion, as well as sample breadth applied to the mucous sintering for PwG panels, and it has been discovered that the optimum heating condition would be 700°C within forty minutes and that the ideal sample proportion as well as PwG breadth would be 5 wt.% as well as 0.8 mm. Elevated-quality white illumination can be produced by straight combining the as-prepared sample into one blue chip while applying one forwarding flux reaching 20 mA. At a CCT of 4696 K, an LE reaching 134.33 lm/W, as well as one CRI reaching 68.5, the WLED has an excellent optic efficiency. These findings suggest that for elevated-energy WLED applications, the examined CGCs can be an exciting replacement for the traditional phosphor/epoxy-resin hue converter.

5. ACKNOWLEDGEMENT

The authors wish to express their gratitude to the Posts and Telecommunications Institute of Technology, Vietnam, for financial support for this research.

REFERENCES

Anh, N. D. Q., N. T. P. Loan, P. V. De, and H. Y. Lee (2025). Potassium Bromide Scattering Simulation for Improving Phosphor-Converting White LED Performance. *Optoelectronics and Advanced Materials - Rapid Communications*, **19**(7-8); 378–383

Anh, N. D. Q. and H. V. Ngoc (2020). Building Superior Lighting Properties for WLEDs Utilizing Two-Layered Remote Phosphor Configurations. *Materials Science-Poland*, **38**(3); 493–501

Camargo, L., P. González, M. Santiago, H. O. Dávila, and J. Marcazzó (2022). A Preliminary Study of the Radioluminescence and Optically Stimulated Luminescence of CaF_2:Ce,Dy Phosphor. *Journal of Luminescence*, **246**; 118845

Chan, J., B. Devakumar, H. Gao, and X. Huang (2024). Efficient Violet-Light-Excitable Blue-Cyan-Emitting $Ca_2YHf_2GaAl_2O_{12}:Ce^{3+}$ Garnet Phosphors Enable High-Color-Rendering Full-Spectrum Warm-White LEDs. *Materials Today Chemistry*, **40**; 102218

Chen, X. and X. Huang (2024). Highly Efficient Blue-Light-Excitable Ultra-Broadband Orange-Emitting $Mg_2 \cdot {}_5Y_1 \cdot {}_5Al_1 \cdot {}_5Si_2 \cdot {}_5O_{12}:Ce^{3+}$ Garnet Phosphors for Solid-State Lighting. *Journal of Alloys and Compounds*, **997**; 174906

Chen, Z., G. Dong, G. Barillaro, J. Qiu, and Z. Yang (2021). Emerging and Perspectives in Microlasers Based on Rare-Earth Ions Activated Micro-/Nanomaterials. *Progress in Materials Science*, **121**; 100814

Chen, Z., G. Dong, H. Gao, and J. Qiu (2019). Two-/Multi-Wavelength Light Excitation Effects in Optical Materials: From Fundamentals to Applications. *Progress in Materials Science*, **105**; 100568

Cong, P. H. and N. D. Q. Anh (2025). Augmenting Chroma Performance for WLED Employing $Sr_8ZnSc(PO_4)_7:Eu^{2+}$@AlAs as a Scattering-Enhancing Substance. *Science & Technology Indonesia*, **10**(2); 467–472

Cong, P. H., L. X. Thuy, N. T. P. Loan, H. Y. Lee, and N. D. Q. Anh (2024). ZnO-Doped Yellow Phosphor Compound for Enhancing Phosphor-Conversion Layer's Performance in White LEDs. *Optoelectronics and Advanced Materials - Rapid Communications*, **18**(7-8); 389–395

Das, A., S. Saha, K. Panigrahi, A. Mitra, R. Chatterjee, U. K. Ghorai, and K. K. Chattopadhyay (2018). Morphology Control and Photoluminescence Properties of Eu^{3+}-Activated $Y_4Al_2O_9$ Nanophosphors for Solid State Lighting Applications. *CrystEngComm*, **20**(18); 2540–2552

Dong, L., L. Zhang, Y. Jia, Y. Xu, S. Yin, and H. You (2020). Realizing Broadband Spectral Conversion in Novel Ce^{3+}, Cr^{3+}, Ln^{3+} (Ln = Yb, Nd, Er) Tridoped Near-Infrared Phos-

phors via Multiple Energy Transfers. *Ceramics International*, **47**(3); 3127–3135

Fang, H. et al. (2025). Reactive Spark Plasma Sintering of YAG–YAG:Ce Composite Phosphor Ceramics for Laser-Driven Lighting with High Luminous Efficacy. *Journal of Materials Chemistry C*, **13**(9); 4781–4790

Fang, Z., R. Cao, F. Zhang, Z. Ma, G. Dong, and J. Qiu (2014). Efficient Spectral Conversion from Visible to Near-Infrared in Transparent Glass Ceramics Containing Ce^{3+}-Yb^{3+} Codoped $Y_3Al_5O_{12}$ Nanocrystals. *Journal of Materials Chemistry C*, **2**(12); 2204–2211

Gong, M., W. c. Xiang, J. Huang, C. Yin, and X. Liang (2015). Facile Synthesis and Optical Properties of Ce:YAG Polycrystalline Ceramics with Different SiO_2 Content. *RSC Advances*, **5**(92); 75781–75786

Hop, D. T. B., T. Q. Tuan, N. Van Quang, N. Tu, H. L. Tien, M. T. Tran, and P. T. L. Huong (2024). Enhanced Visible-Light Photocatalytic Degradation Efficiency of Ce^{3+}-Doped ZnO Nanoparticles Synthesized by Sol-Gel Method. *Ceramics International*, **50**(10); 17338–17353

Hu, Y., Z. Li, and W. Pan (2018). Sandwich-Like Transparent Ceramic Demonstrates Ultraviolet and Visible Broadband Downconversion Luminescence. *RSC Advances*, **8**(24); 13200–13204

Huang, J., X. Hu, J. Shen, D. Wu, C. Yin, R. Xiang, and W. Xiang (2015). Facile Synthesis of a Thermally Stable Ce^{3+}:$Y_3Al_5O_{12}$ Phosphor-in-Glass for White LEDs. *CrystEngComm*, **17**(37); 7079–7085

Huang, X., J. Chan, and X. Chen (2024). A Well-Performed Green-Emitting $Lu_1 \cdot {}_5Ca_1 \cdot {}_5Al_3 \cdot {}_5Si_1 \cdot {}_5O_{12}$:$Ce^{3+}$ Garnet Phosphor for High-Quality pc-WLEDs. *Ceramics International*, **50**(24); 55979–55986

Jiang, Z. et al. (2025). Growth and Photoluminescent Performance of Ce:YAG Single Crystal for High-Power w-LEDs Application. *Optical Engineering*, **64**(11); 117102

Kumar, M. and P. Kumar (2024). *White Light Emitting Materials: Illuminating Brilliance*, volume 31 of *Progress in Optical Science and Photonics*. Springer Nature Singapore, Singapore

Le, P. X., S. D. Ho, N. D. Q. Anh, and H.-Y. Lee (2021). Triple-Layer Remote Phosphor Structure: A Potential Packaging Configuration to Enhance Both Color Quality and Lumen Efficiency of 6,000–8,500 K WLEDs. *Materials Science-Poland*, **39**(4); 458–466

Li, X., H. Guo, X. Liu, R. Wei, F. Hu, and S. Zhou (2019). A New Parameter for Characterizing Eu^{3+} Distribution in Mixed-Valence Eu-Doped Cubic LaF_3-Based Transparent Glass-Ceramics. *Journal of the American Ceramic Society*, **102**(11); 6640–6648

Li, X., Y. Li, L. Wang, J. Kang, and J. Zou (2024). Luminescence Saturation Studies of YAG:Ce Phosphor Ceramics for White Laser Diode Lighting. *Journal of Materials Science: Materials in Electronics*, **35**(4); 299

Lin, H., B. Wang, J. Xu, R. Zhang, H. Chen, Y. Yu, and Y. Wang (2014). Phosphor-in-Glass for High-Powered Remote-Type White AC-LED. *ACS Applied Materials & Interfaces*, **6**(23); 21264–21269

Liu, B. et al. (2025). Impact of Ce^{3+} Concentration and Thickness on Luminance and Chromaticity Uniformity of YAG:Ce Ceramic Color Converters for Laser Lighting. *Ceramics International*, **51**(29); 61285–61292

Liu, Z. et al. (2024). Laminated Composite of Ceramic/Glass Films to Realize High Luminous Efficiency and High Color Quality in Laser-Driven White Lighting. *Journal of Materials Chemistry C*, **12**(31); 11898–11906

Long, Y., J. Li, Z. Fang, and B. Guan (2020). Modulation of Activator Distribution by Phase-Separation of Glass for Efficient and Tunable Upconversion Luminescence. *RSC Advances*, **10**(21); 12217–12223

Lü, W., M. Jiao, B. Shao, L. Zhao, Y. Feng, and H. You (2015). An Intense NIR Emission from $Ca_{14}Al_{10}Zn_6O_{35}$:$Mn^{4\equiv}$,Yb^{3+} via Energy Transfer for Solar Spectral Converters. *Dalton Transactions*, **45**(2); 466–468

Lv, Y., L. Wang, Y. Zhuang, T. Zhou, and R. Xie (2017). Discovery of the Yb^{2+}–Yb^{3+} Couple as Red-to-NIR Persistent Luminescence Emitters in Yb-Activated $(Ba_{1-x}Sr_x)AlSi_5O_2N_7$ Phosphors. *Journal of Materials Chemistry C*, **5**(28); 7095–7101

Ma, Y. et al. (2024). New Phase-Construction Phosphors Ceramics for Warm-White Solid-State Lighting: Orange-Yellow-Emitting $(Lu,Gd)_3(Sc,Al)_5O_{12}$:Ce^{3+}. *Ceramics International*, **50**(23); 49643–49651

Markovskyi, A., V. Gorbenko, S. Nizhankovskiy, T. Zorenko, A. Fedorov, and Y. Zorenko (2024). Two-Layered $Lu_3Al_5O_{12}$:Ce/$Y_3Al_5O_{12}$:Ce Composite Phosphor Converter for White Light-Emitting Diode Devices. *Optical Materials: X*, **22**; 100329

Meejitpaisan, P., R. Doddoji, S. Kothan, and J. Kaewkhao (2022). Photo and X-Ray Luminescence Characteristics of CeF_3-Doped SiO_2 + B_2O_3 +AlF_3 + NaF + CaF_2 Scintillating Glasses. *Radiation Measurements*, **158**; 106853

Milisavljevic, I., M. J. Pitcher, J. Li, S. Chenu, M. Allix, and Y. Wu (2022). Crystallization of Glass Materials into Transparent Optical Ceramics. *International Materials Reviews*, **68**(6); 648–676

Motloung, S., F. Dejene, R. Kroon, H. Swart, and O. Ntwaeaborwa (2015). Radiative Energy Transfer in $ZnAl_2O_4$:0.1% Ce^{3+}, x% Eu^{3+} Nanophosphor Synthesized by Sol–Gel Process. *Physica B: Condensed Matter*, **468–469**; 11–20

My, L. T. T., N. L. Thai, T. M. Bui, H.-Y. Lee, and N. D. Q. Anh (2022). Phosphor Conversion for WLEDs: YBO_3:$Ce^{3\equiv}$,Tb^{3+} and Its Effects on the Luminous Intensity and Chromatic Properties of Dual-Layer WLED Model. *Materials Science-Poland*, **40**(4); 105–113

Pathak, A., R. Talewar, C. Joshi, and S. Moharil (2016). Sensitization of Yb^{3+} Emission in $CaYAl_3O_7$ Host. *Optical Materials*, **64**; 217–223

Qiang, Y. et al. (2025). BaO-Y_2O_3-Al_2O_3-SiO_2/YAG:Ce: A Novel YAG:Ce Glass-Ceramic with Excellent Fluorescent Properties for Phosphor-Converted White LEDs. *Ceramics*

International, **51**(14); 19199–19210

Qin, Y., Y. Cao, L. Ning, X. Wang, and Y. Wang (2024). Unraveling the Defect-Induced Spectral Tuning in a Ce-Doped Garnet Solid-Solution Phosphor. *Laser & Photonics Reviews*, **18**(10); 2400347

Samanta, T., S. Sarkar, V. N. K. B. Adusumalli, A. E. Praveen, and V. Mahalingam (2015). Enhanced Visible and Near Infrared Emissions via Ce^{3+} to Ln^{3+} Energy Transfer in Ln^{3+}-Doped CeF_3 Nanocrystals (Ln = Nd and Sm). *Dalton Transactions*, **45**(1); 78–84

Shen, X., H. Chen, M. Xu, X. Ji, and Q. Qin (2024). Measurement Model of Circadian Action Factor of Phosphor-Converted White LEDs Based on Photometric, Electrical, and Thermal Properties. *Metrologia*, **61**(2); 025002

Shrivastava, R. and R. S. Kundu (2023). Studies on Photoluminescence and Thermoluminescence Properties of Yttrium Aluminium Perovskite (YAP-$YAlO_3$) Doped with Cerium(III). *Chemical Papers*, **77**(11); 7155–7161

Tang, L., H. Ye, and D. Xiao (2018). Photo-Induced Luminescence Degradation in Ce, Yb Co-Doped Yttrium Aluminum Garnet Phosphors. *Applied Optics*, **57**(26); 7627–7631

Tran, T. C., N. D. Q. Anh, and N. T. P. Loan (2020). Comparison of Calcium Carbonate and Titania Particles on Improving Color Homogeneity and Luminous Flux of WLEDs. *Telkomnika*, **18**(5); 2690–2696

Tung, H. T., N. D. Q. Anh, and H. Y. Lee (2024). Impact of Phosphor Granule Magnitudes as Well as Mass Proportions on the Luminous Hue Efficiency of a Coated White Light-Emitting Diode and One Green Phosphor Film. *Optoelectronics and Advanced Materials - Rapid Communications*, **18**(1-2); 58–65

Wang, G. et al. (2024). Innovative Architecture for Phosphor-in-Glass Films Enabling Superior Luminance and Color Quality Laser-Driven White Light. *Laser & Photonics Reviews*, **18**(6); 2301263

Wang, H., S. Ye, S. Li, T. Liu, J. Lin, and D. Wang (2015). Broadband Down-Conversion Through the Co-Contribution of Simultaneous Energy Transfer from $Eu^{3}\equiv/_{2}^{+}$ to Yb^{3+} and CTS Absorption of Yb^{3+}. *Journal of Alloys and Compounds*, **648**; 13–17

Wang, S., Q. Sun, B. Li, H. Guo, and X. Huang (2018). High-Efficiency and Thermal-Stable Tunable Blue-Green-Emitting $Ca_3Lu(AlO)_3(BO_3)_4$:$Ce^{3}\equiv$,Tb^{3+} Phosphors for Near-UV-Excited White LEDs. *Dyes and Pigments*, **157**; 314–320

Wei, Y., H. Ebendorff-Heidepriem, and J. Zhao (2019). Recent Advances in Hybrid Optical Materials: Integrating Nanoparticles Within a Glass Matrix. *Advanced Optical Materials*, **7**(21); 1900702

Won, H., H. Nersisyan, C. Won, and K. Lee (2011). Effect of Metal Halide Fluxes on the Microstructure and Luminescence of $Y_3Al_5O_{12}$:Ce^{3+} Phosphors. *Materials Chemistry and Physics*, **129**(3); 955–960

Xu, Z., R. Zhang, X. Qin, and S. Wang (2024). Translucent YAG:Ce-SiO_2 Composites Prepared by Pressureless Sintering: Structures, Luminescence Properties, and Applications in the White LEDs/LDs. *ACS Applied Optical Materials*, **2**(6); 1136–1143

Yan, Y., Z. Chen, X. Jia, and S. Li (2017). Photoluminescence Properties of Mn^{2+}/Yb^{3+} Co-Doped Oxyfluoride Glasses for Solar Cells Application. *Optical Materials*, **75**; 465–470

Yue, K., Z. You, P. Ke, J. Wen, M. Jia, and T. Wang (2022). Visible to Near Infrared Energy Transfer in Ce^{3+}, Yb^{3+} Co-Doped YAG Crystal Prepared by the Co-Precipitation Method. *Optical Materials Express*, **12**(2); 653–665

Zeng, H., T. Chen, Y. Guo, and X. Wu (2025). Yttrium Aluminum Garnet Fluorescent Conversion Films for Solid-State Lighting: Interface Reaction Synthesis Strategy and Modulation of Warm White Light. *Dalton Transactions*, **54**(9); 3930–3938

Zhang, B. et al. (2024). Robust High-Efficiency LuAG:Ce Phosphor-in-Silica Glass (PiSG) for High-Brightness Laser Lighting. *Ceramics International*, **50**(3); 5868–5876

Zhao, J., C. Guo, T. Li, D. Song, and X. Su (2015). Near-Infrared Down-Conversion and Energy Transfer Mechanism in Yb^{3+}-Doped $Ba_2LaV_3O_{11}$ Phosphors. *Physical Chemistry Chemical Physics*, **17**(39); 26330–26337

Zhao, W., C. Mancini, D. Amans, G. Boulon, T. Epicier, Y. Min, and A. Yoshikawa (2010). Evidence of the Inhomogeneous Ce^{3+} Distribution Across Grain Boundaries in Transparent Polycrystalline Ce^{3+}-Doped $(Gd,Y)_3Al_5O_{12}$ Garnet Optical Ceramics. *Japanese Journal of Applied Physics*, **49**(2R); 022602

Zhou, C. et al. (2024). MAS:Eu-YAG:Ce Composite Phosphor Converters with Excellent Thermal Performance and Enhanced Color Rendering Index for High-Power White LDs. *Ceramics International*, **50**(14); 25908–25917

Zhu, C., D. Wu, Y. Zhang, M. Zhang, and Y. Yue (2015). Composition Dependence of the Optical and Structural Properties of Eu-Doped Oxyfluoride Glasses. *Journal of Alloys and Compounds*, **632**; 291–295

